Relation between the geometry of rail welds and the dynamic wheel–rail response: numerical simulations for measured welds

M J M M Steenbergen* and **C Esveld**
Faculty of Civil Engineering and Geosciences, Railway Engineering, Delft University of Technology, Delft, The Netherlands

Abstract: The primary mechanisms playing a role in the dynamic wheel–rail response to rail weld irregularities in a ballasted track are pointed out. The concept of P_1 and P_2 forces for metallurgical rail welds, introduced in a first paper [**1**] concerning the present research, is further elaborated. The dynamic wheel–rail response is simulated for a number of geometrical rail weld measurements. Results show a good correlation between the gradient of the rail weld geometry and the maximum dynamic wheel–rail contact forces, whereas the correlation with vertical peak deviations is shown to be very poor. Therefore, an assessment method based on the gradient (introducing a speed-dependent quality index [**1**]) is more consistent than a method based on vertical tolerances. An approximate formula is presented to calculate the maximum dynamic wheel–rail contact force as a function of the train velocity and the maximum gradient of the weld geometry, in analogy to Jenkins' formulae for calculating P_1 and P_2 forces at dipped rail joints.

Keywords: rail welds, welding, weld geometry, rail joints, dynamic wheel–rail forces

1 INTRODUCTION

The lifetime of rails in continuously welded rail (CWR) tracks is often determined by the welds, which form the weakest spots in the rail. This is due to several reasons. First, their vertical geometry is worse than the initial geometry of the rest of the rail, leading to local dynamic amplifications of the wheel–rail contact force. Further, the cross-section is not constant along the rail (especially for *in situ* made thermit welds), causing stress concentrations that lead to crack initiation and propagation and finally to failure (especially in the area with tensile stresses). These effects are amplified by the fact that the rail material is inhomogeneous in the longitudinal direction because of the difference between the parent and the weld material and the possible inclusion of contaminations. Here, also the heat-affected zone and the resulting hardness profile of the rail surface play a role. Finally, the residual stress state in the welded rail in combination with the axial tensile stresses as a result of changing ambient temperatures during winter may lead to early damage.

The fatigue crack growth in a welded rail under the influence of residual stresses was studied by Skyttebol *et al.* [**2**]. In this study, it was also found that typical crack sizes in welds can lead to failure in a relatively short time if the residual stress field interacts with the axle load. This is the case if dynamic amplifications of the axle load occur because of a bad geometry of the weld. Mutton and Alvarez [**3**] studied the failure modes in aluminothermic (thermit) welds under high axle load conditions and also carried out some experimental investigations into the relation between the longitudinal weld profile, the dynamic load amplification factor (DAF), and the train speed.

**Corresponding author: Faculty of Civil Engineering and Geosciences, Railway Engineering, Delft University of Technology, Section of Road and Railway Engineering, PO Box 5048, NL 2600 GA Delft, The Netherlands. email: m.j.m.m. steenbergen@tudelft.nl*

For the reasons explained earlier, the lifetime of rails in CWR tracks can be significantly extended by adopting an adequate assessment method for the welds. Steenbergen and Esveld [1] presented a theoretical model to estimate the maximum dynamic wheel–rail contact forces occurring at the rail welding surface irregularities. Further, on the basis of this model, an assessment method for vertical rail weld geometry was presented, based on the limitation of the gradient of the discrete measurement signal. The weld quality index (QI) has been introduced as the ratio of the maximum absolute value of the gradient (on 25 mm basis) of an actual weld measurement to the speed-dependent norm value. It was shown that a linear relationship between the dynamic wheel–rail force and the QI exists in theory. Given the fact that the rate of track deterioration is determined by the level of dynamic contact forces, a weld assessment based on the QI is consistent in a life-cycle approach.

The aim of this article is to validate the model and the theory presented in reference [1] with the help of numerical simulations of the dynamic wheel–rail contact force. In order to perform this validation, the vertical geometry along the rail of 239 rail welds has been measured, after which the dynamic wheel–rail response was calculated for each of them.

2   MODEL FOR SIMULATION OF DYNAMIC WHEEL–RAIL INTERACTION AT RAIL WELDS

The simulations have been performed with the FE-package DARTS-NL [4]. An overview of the model is given in Fig. 1.
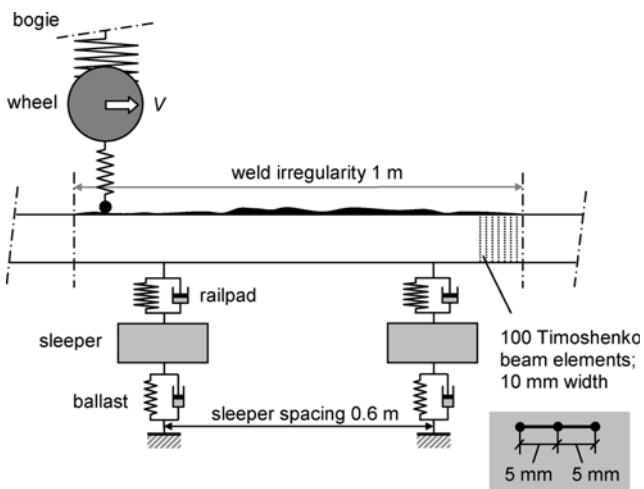

Fig. 1   FE model for simulation of the wheel–rail interaction at rail weld surface irregularities

The measured irregularity has a sampling interval of 5 mm and a total length of 1 m. In the model, the rail is divided into beam elements with a length of 10 mm; therefore, each element has three vertical coordinates. The irregularity is centred in the middle of a sleeper span, where the weld is made in practice. The model uses a non-linear Hertzian contact model. The time step in the calculations is taken as the ratio of the element size to the train velocity (a reduction of this time step by 50 per cent leads to deviations in the results within a margin of 3 per cent). A large number of sleeper bays are included, with non-reflective boundaries at both ends. The number of sleeper bays is, however, not very relevant, given the local effect of the weld irregularity.

3   PRIMARY MECHANISMS IN THE DYNAMIC WHEEL–RAIL RESPONSE TO RAIL WELD IRREGULARITIES AND THEIR RELATION TO TRACK DETERIORATION

In reference [1], the concept of P_1 and P_2 forces for metallurgical rail welds was introduced, in analogy to the terminology for bolted joints or insulated rail joints (non-welded joints). It was shown that the P_1 force, which has, in general, a relatively high frequency, can be attributed to the quasi-instantaneous reaction of the track to the irregularity, whereas the P_2 force with a relatively low frequency can be attributed to the delayed reaction of the axle, which has a much larger inertia relative to the track.

In Fig. 2, simulation results of the dynamic wheel–rail response are shown when a train passes an artificial weld irregularity in the track. A similar case was shown in reference [1] for a smooth irregularity; here also a non-smooth irregularity is taken into account to cover all the elementary possibilities in the surface of real rail welds. The considered artificial weld includes a smooth irregularity with a longer length scale (a harmonic wave with a length of 1 m and a top value of 1 mm) and a non-smooth irregularity with a short length scale (a triangular peak with a basis of 100 mm and a top of 0.2 mm). The simulation has been performed with the model shown in Fig. 1. The following parameter values have been adopted in the calculation: a train speed V of 140 km/h; a wheel mass (half un-sprung mass) of 970 kg; a sleeper mass of 300 kg; UIC 54 rail; a primary suspension stiffness of 1.8×10^6 N/m (per wheel); a railpad stiffness of 1.2×10^9 N/m; and a ballast stiffness of 30×10^6 N/m per sleeper, where the latter value is rather small, to account for the generally high degree of looseness of the sleepers close to the irregularity.
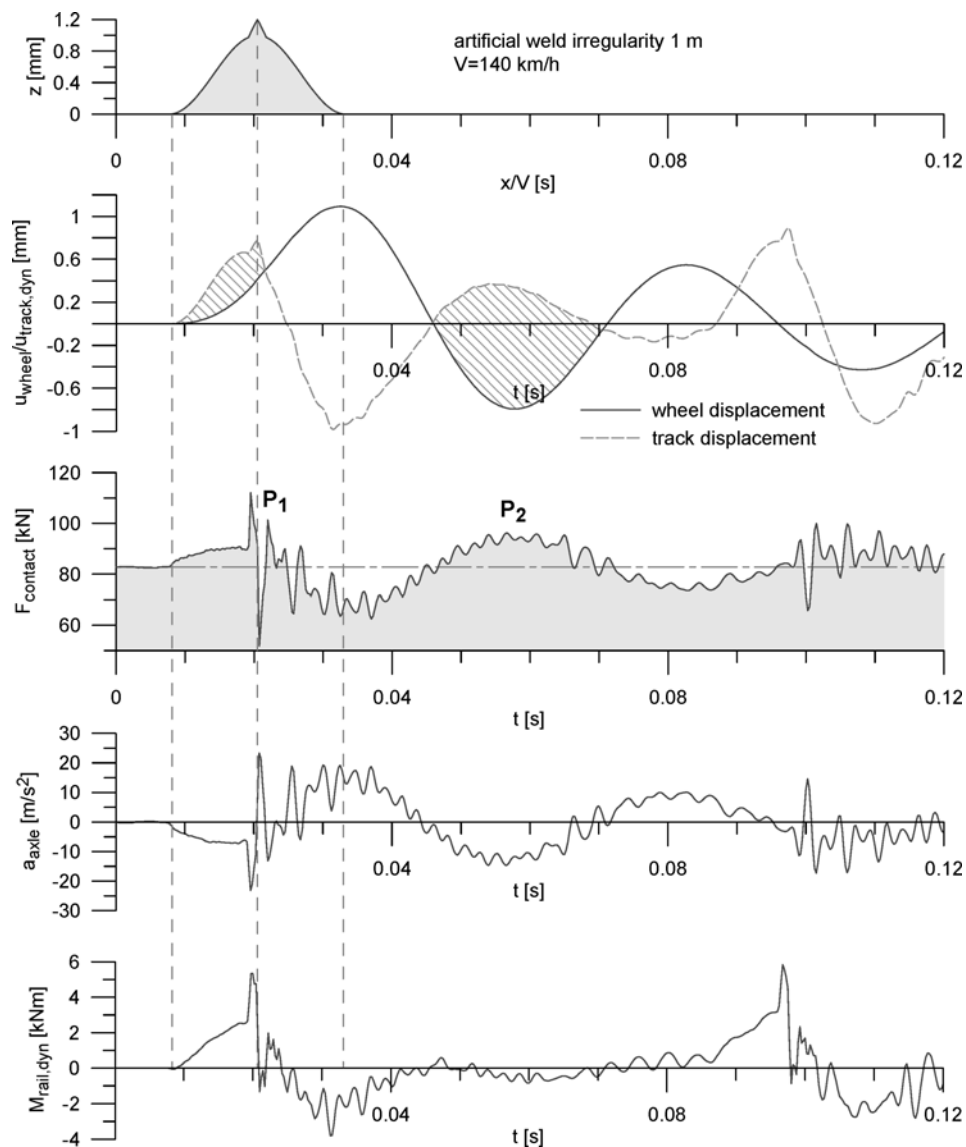
Fig. 2 Dynamic response of the wheel–rail system to an artificial weld with both long and short length scale irregularities

In Fig. 2, the following quantities are shown as a function of time:

(a) the geometry of the irregularity z;
(b) the dynamic part of the vertical wheel displacement u_{wheel} of the first wheel of a passing bogie, defined positive in the upward direction and calculated in a convective reference frame moving along with the wheel;
(c) the dynamic part of the displacement $u_{track,dyn}$ of the rail/track, calculated in a fixed coordinate system with its origin at the centre of the irregularity and defined positive in the downward direction;
(d) the wheel–rail contact force F_{dyn} for the concerned wheel (the dynamic force is

superimposed on the static value), in a convective reference frame;
(e) the axle box acceleration a_{axle}, in a convective reference frame;
(f) the dynamic part of the bending moment in the rail $M_{rail,dyn}$, in a fixed coordinate system at the centre of the irregularity.

From Fig. 2, a number of observations can be made. They are as follows.

1. The track follows the vertical irregularity quasi-instantaneously; especially for the short-length irregularity, this is clearly visible. The wheel displacement shows a delay in response relative to the track. It does not show any influence of the short peak in the irregularity, whereas this peak
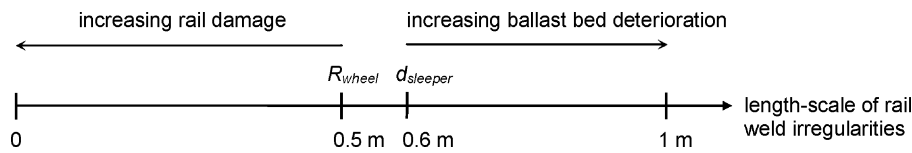
Fig. 3 Types of deterioration of the track system dependent on the length scale of the rail welding surface irregularities

is reproduced almost exactly in the rail displacements.

2. The maximum dynamic contact force is determined by the irregularity with the shortest length scale. However, the corresponding force peaks are rather narrow and the corresponding amount of energy is rather small. These high-frequency peak forces damage mostly the rail itself (causing fatigue), as can be seen also in the graph of the dynamic bending rail moments. The related energy will vanish by wave propagation in the rail and by dissipation in, mainly, the railpads.

3. The highest energy of the dynamic contact force is contained in the 'carrier frequency', which can be clearly observed. This carrier frequency is related to the delayed reaction of the wheel mass to the irregularity (the P_2 force). The relatively large energy contained in the relatively low carrier frequency is mainly responsible for ballast bed deterioration, as it is not efficiently dissipated in the rail and the railpads.

Globally speaking, the components of irregularities with a longer length scale than the wheel radius or the sleeper span (0.5–0.6 m) damage the ballast bed, whereas the components with a shorter length scale damage the railhead and rail (Fig. 3).

4 SIMULATIONS OF THE DYNAMIC WHEEL–RAIL RESPONSE AT MEASURED RAIL WELD IRREGULARITIES

In order to perform the simulations of the dynamic wheel–rail response at rail welding irregularities, the vertical geometry of 239 arbitrary welds has been measured on the Dutch network. The cumulative distribution function of the extreme value of the gradient (on 25 mm basis, [1]) of the set of measurements is shown in Fig. 4, where the gradient norm value 1.8 mrad at 140 km/h is also indicated.

In Fig. 5, the simulation results are shown for the maximum absolute values of the dynamic wheel–rail contact forces (during the time interval that a train wheel passes the weld) for the weld population, plotted as a function of the maximum absolute values of gradient of the weld geometry, on a 5 mm (the sampling interval) and a 25 mm basis (the

sampling interval after averaging, see reference [3]), respectively.

The following parameter values have been adopted in the calculation: a wheel mass (half un-sprung mass) of 970 kg; a sleeper mass of 300 kg; UIC 54 rail; a primary suspension stiffness of 1.8×10^6 N/m (per wheel); a railpad stiffness of 1.2×10^9 N/m; and a ballast stiffness of 78×10^6 N/m per sleeper. The static wheel load has been taken as 82 kN.

In both graphs in Fig. 5, a linear regression line is displayed, calculated using a least-squares method. The value of R^2 (the coefficient of determination) is a measure of the goodness of fit: 0 indicating no correlation and 1 a perfect correlation. Alternatively, it is defined as the proportion of the variance of one variable that is predictable by the other one. It is remarked that a regression line does not pass necessarily through the origin. However, the better the model [1] predicts the calculation results, the closer the regression line will be to a linear fit through the origin, as for a zero gradient also the dynamic effects should vanish. R^2 is the squared value of the linear correlation coefficient r ($-1 \leqslant r \leqslant 1$), which quantifies the linear association (both the strength and the direction) between the two variables.

Figure 5 shows a very good correlation (0.91) between the maximum dynamic wheel–rail contact forces and the maximum gradient of the measurement signal on a 5 mm basis. When plotting the maximum forces as a function of the gradient of
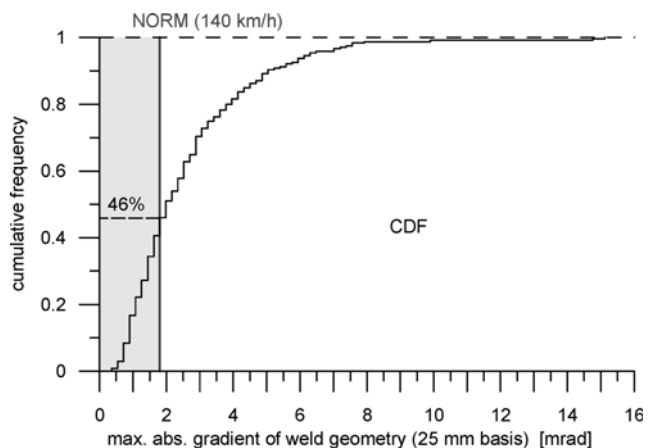

Fig. 4 Cumulative distribution of the sample of 239 rail welds used for the simulations
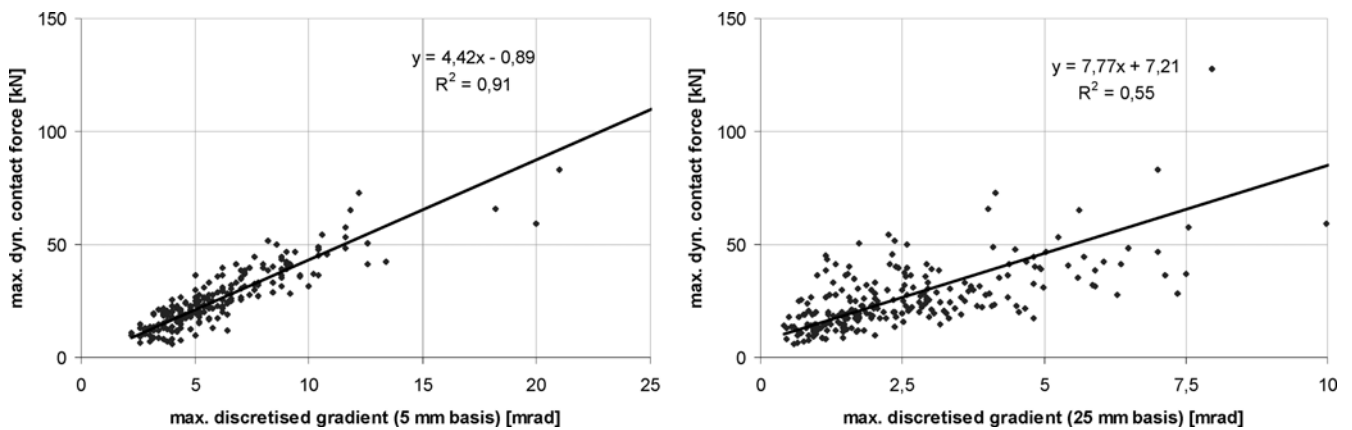
Fig. 5 Maximum dynamic wheel–rail contact forces as a function of the maximum absolute value of the discrete gradients of the weld population, on 5 and 25 mm basis, respectively, for a train speed of 140 km/h

the averaged signal on a 25 mm basis, the correlation decreases to 0.55. This drop is related to the phenomenon shown in Fig. 2: the irregularities in the signal with the shortest length scale generate the highest contact forces, but the corresponding peaks are rather narrow. This also implies that the maximum force when filtered (with a low-pass filter with a cut-off frequency given by the ratio of the train speed to the minimum wavelength of the averaged signal) would show a much better correlation with the gradient on 25 mm basis, comparable with the correlation value found for the gradients on a 5 mm basis. Alternatively, it may be stated that the maximum dynamic contact force correlates well and linearly with the maximum gradient of the weld geometry, when these maxima are taken in the same frequency band.

Figure 6 shows the maximum dynamic wheel–rail contact forces as a function of the maximum absolute values of the second derivatives taken on a 5 mm basis. The correlation is good. Also here, the

correlation drops to 0.56 when the second derivatives are taken on a 25 mm basis (data not shown). The graph at the right in Fig. 6 shows the correlation between the maximum dynamic forces and the vertical peak deviations of the welds. R^2 is close to zero, from which it can be concluded that there is no correlation at all.

Generally, it may be concluded that the maximum gradient gives a good indication of the maximum dynamic force occurring for the weld under consideration. Therefore, the QI is a suitable tool to assess the rail weld geometry from a viewpoint of the dynamic wheel–rail response. Further, an assessment based on the principle of vertical peak deviations, which should not exceed given tolerances, is inadequate to assess the rail welds from the viewpoint of dynamic wheel–rail forces and the resulting track deterioration.

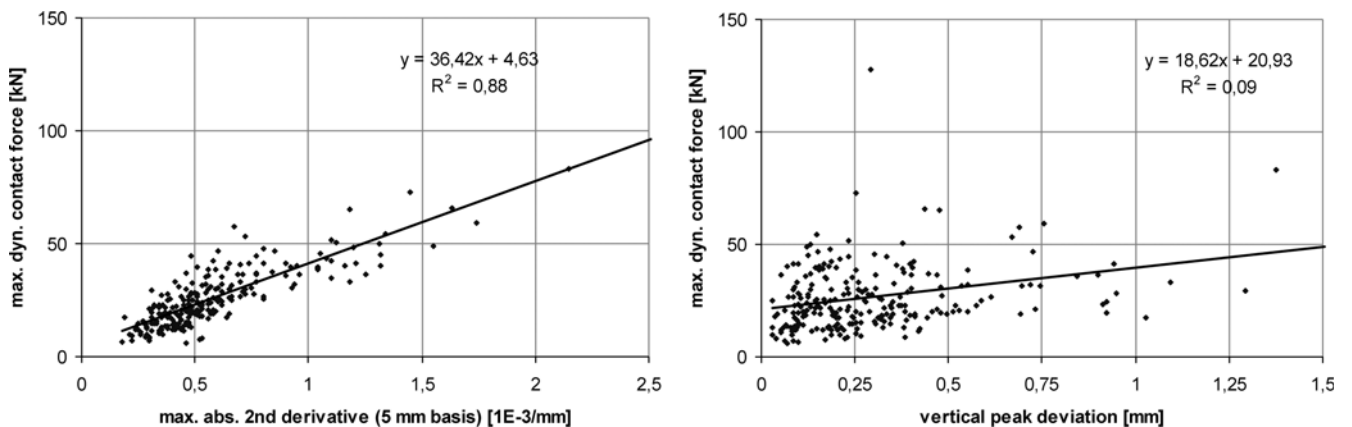The simulations of the dynamic wheel–rail response have been performed for different train

Fig. 6 Maximum dynamic wheel–rail contact forces as a function of the maximum absolute value of the second derivatives of the weld population on 5 mm basis and the peak deviation (on 1 m basis), respectively, for a train speed of 140 km/h

velocities. The main simulation results are summarized in Figs 7 to 10, for the velocities 40, 80, 140 (conventional lines), and 300 km/h (high-speed lines), respectively. In all graphs, the linear regression lines are shown along with their equations. All quantities have been determined for the time interval that a train wheel passes the weld (with a length of 1 m). From Figs 7 to 10, a number of conclusions can be drawn, which are discussed in the following.

The maximum wheel displacement shows a very good correlation with the peak deviation of the weld geometry. This correlation decreases with the train speed: R^2 ranges from 0.95 at 40 km/h to 0.88 at 300 km/h. The respective equations of the linear fits show that at 40 km/h, the relation is almost directly proportional. At 80 km/h, the relation is more than directly proportional, at 140 km/h less, and at 300 km/h much less than directly proportional. Obviously, at 80 km/h, the frequencies corresponding to the wavelengths in the spectra of the welds are close to a resonant frequency of the wheel system, whereas at 140 and 300 km/h, this is not the case. The correlation between maximum wheel displacements and maximum gradients is very bad, R^2 being equal to or smaller than 0.25 for all velocities.

The maximum dynamic rail deflection generally shows a good correlation with the vertical peak deviation of the weld geometry. The correlation increases with the train speed, with values 0.54, 0.92, 0.95, and 0.96 for 40, 80, 140, and 300 km/h, respectively. The equations of the linear fits show that the relationship between the maximum dynamic rail deflections and the peak deviations of the weld geometry can be assumed directly proportional in a good approximation. Only at 40 km/h (where the correlation is rather bad), the relationship is much less than directly proportional. The above justifies the assumption that was made in the modelling of the wheel–rail contact in reference [1], according to which the track follows the vertical rail irregularity quasi-instantaneously and quasi-statically. Only for low train velocities, the model is not accurate, and its use therefore has no theoretical basis in this domain.

Maximum dynamic wheel–rail contact forces generally show a good correlation with the gradient. In Figs 7 to 10, the gradients are taken on a 25 mm basis, as in the definition of the QI. As has been shown in the beginning of this paragraph, the correlation increases significantly when the gradient is taken on a 5 mm basis (to 0.71 at 40 km/h; to 0.78 at 80 km/h; and to 0.91 at 140 km/h; only at 300 km/h, the value drops to 0.77 because of the high velocity of the wheel mass). Alternatively, it would increase when the maximum force is taken

after filtering. Figures 7 to 10 show that the correlation with the gradients increases with the speed. Given the static wheel load of 82 kN, the DAF generally does not exceed a factor of 2. This corresponds to the experimental results of reference [3]. The correlation of the maximum forces with the peak deviations of the weld geometry is very bad; below or equal to 0.17 for all velocities.

Generally, the maximum dynamic rail bending moments correlate much better with the gradient than with the peak deviation. R^2 increases with the velocity, up to 0.91 at 300 km/h. The same holds for the maximum dynamic rail shear forces. Also here, R^2 increases with the velocity. For both moments and shear forces, taking the gradient on a 5 mm basis or filtering the moments and shear forces increases the correlation significantly. At 40 km/h, R^2 increases to 0.64 and 0.61, respectively; at 80 km/h to 0.59 and 0.69; at 140 km/h to 0.76 and 0.83; and only at 300 km/h, R^2 decreases, because of the high value of the velocity, to 0.66 and 0.71, respectively.

Figures 7 to 10 do not show the dynamic wheel–rail response as a function of second derivatives. Generally, the coefficient of determination is comparable with the one obtained with the gradients (0.73, 0.78, 0.88, and 0.58, respectively, for the contact forces at the four analysed velocities, using a 25 mm basis). This is due to the good correlation between gradients and second derivatives of the weld measurements. Figure 11 shows the correlation between the geometrical properties of these measurements. The left plot shows the vertical peak deviations as a function of the maximum gradients (on 25 mm basis), whereas the right plot shows the maximum second derivatives (in absolute sense) as a function of these gradients. The coefficient of determination for the latter relationship is 0.85. The linear fit through the origin coincides in a very good approximation with the line

$$\frac{\mathrm{d}^2}{\mathrm{d}x^2} z_i = \frac{1}{2d} \left| \frac{\mathrm{d}z}{\mathrm{d}x} \right|_{\mathrm{norm}} \tag{1}$$

which was established in reference [1] (Fig. 11) as the central relationship between first and second derivatives. However, the bandwidth for the second derivative as a function of the first derivative, in this figure, concerns the actual value of the second derivative as a function of a limited first derivative and not its extreme value; therefore, it is not applicable here.

The left plot in Fig. 11 shows a wedge-shaped relationship, with an upper bound and a lower bound. The upper bound of the vertical deviation, in absolute sense and as a function of the maximum
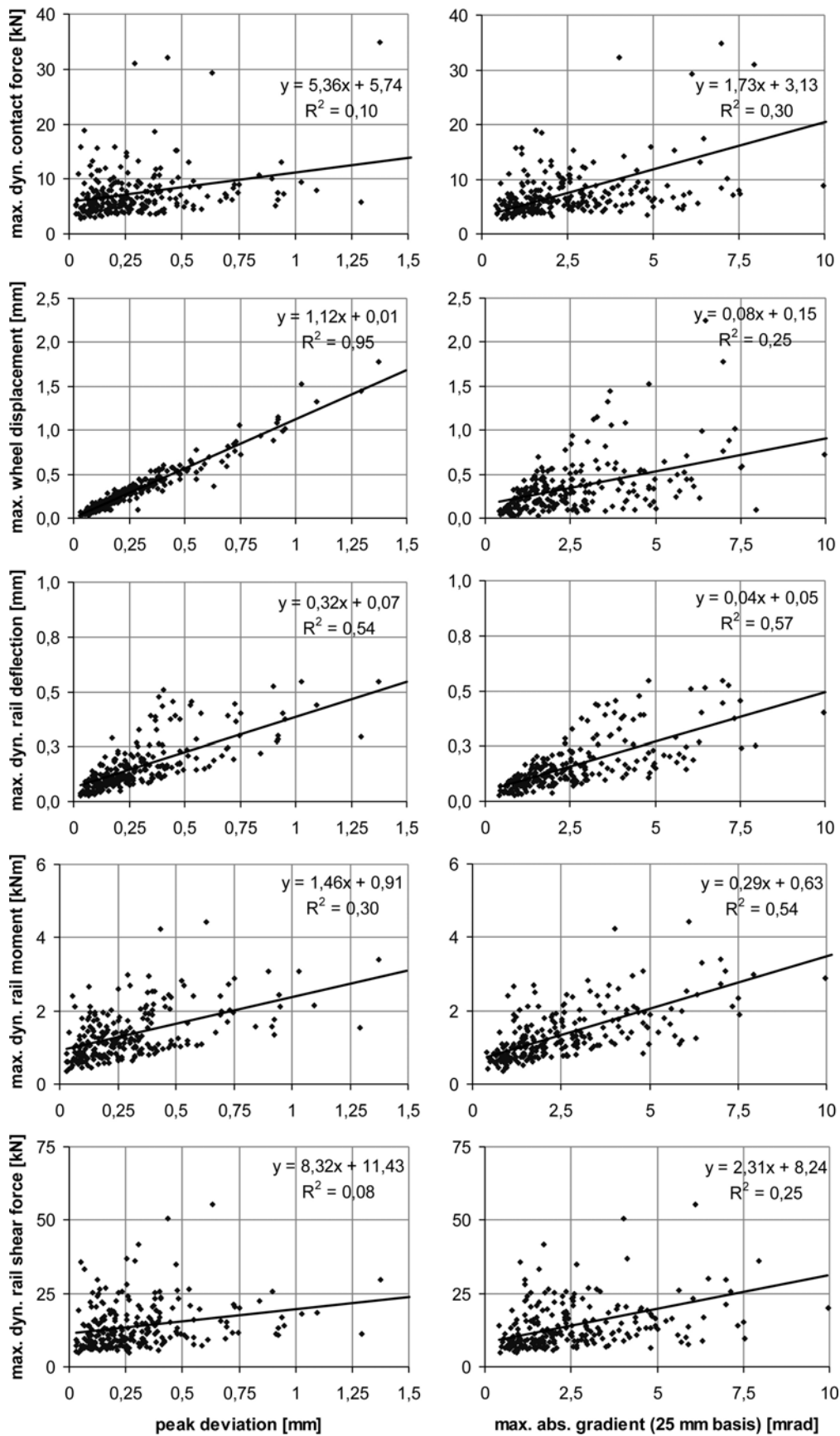
Fig. 7 Dynamic response of the wheel–rail system to rail welding irregularities for a train velocity of 40 km/h
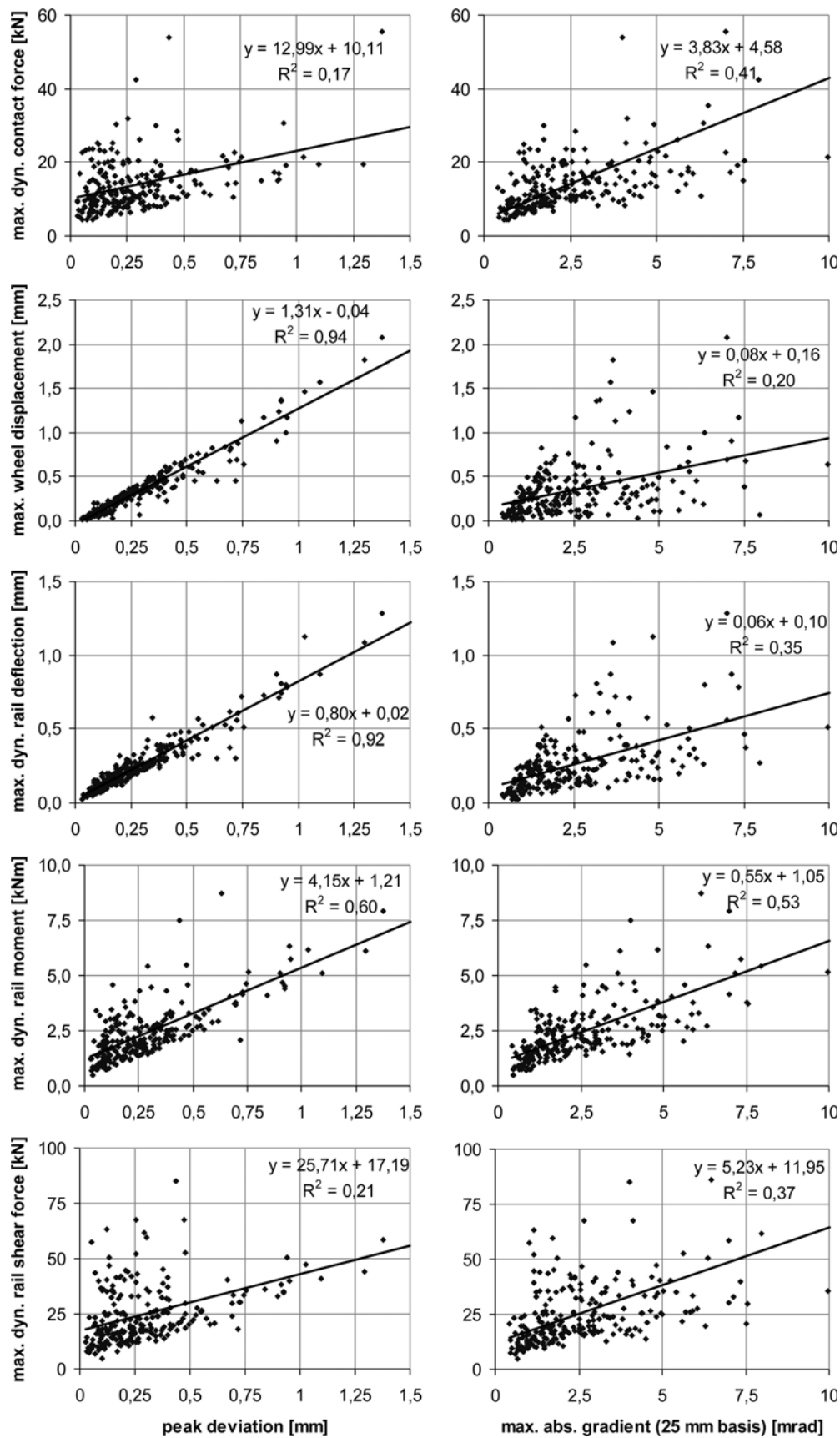
Fig. 8 Dynamic response of the wheel–rail system to rail welding irregularities for a train velocity of 80 km/h
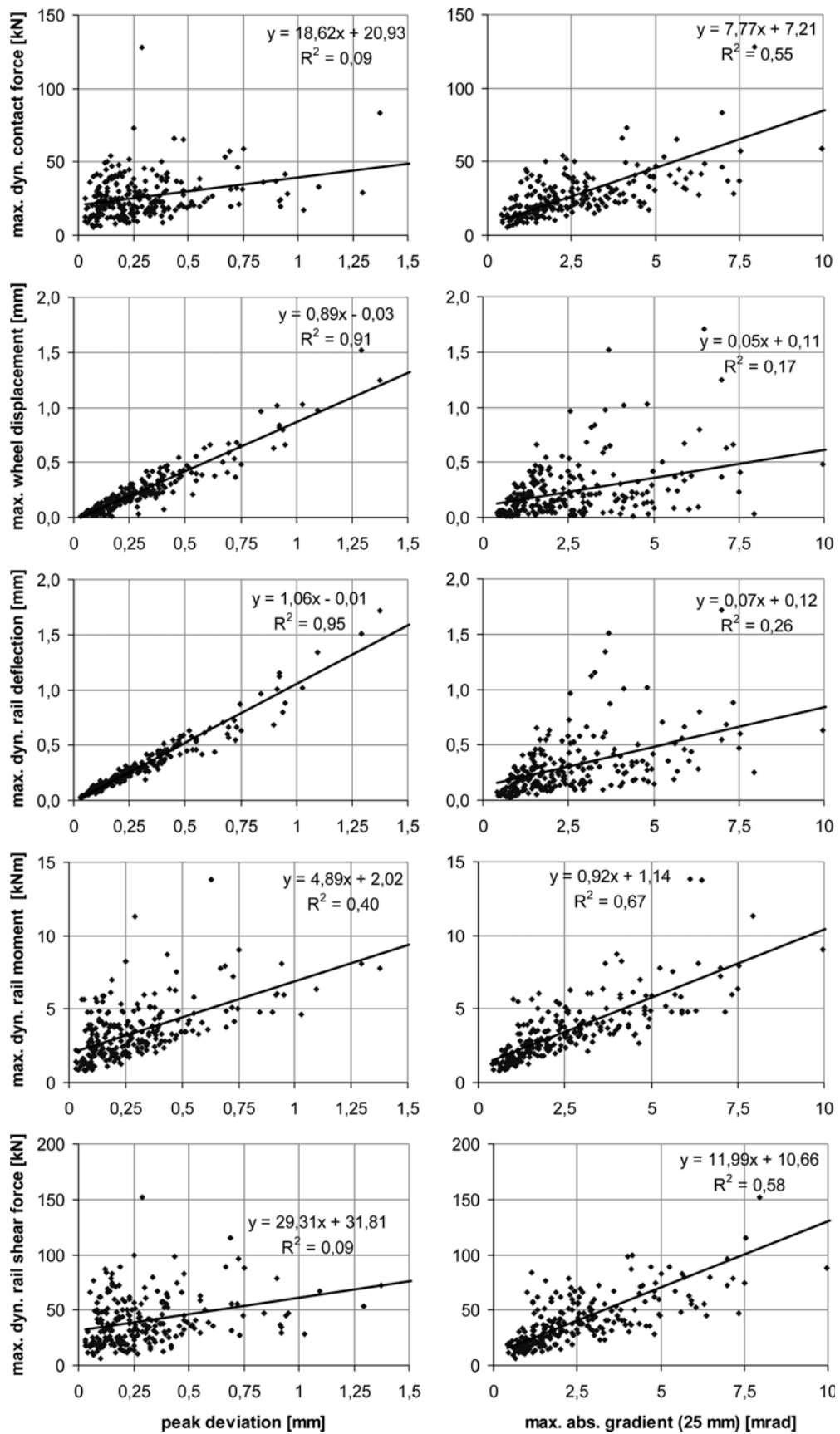
Fig. 9 Dynamic response of the wheel–rail system to rail welding irregularities for a train velocity of 140 km/h
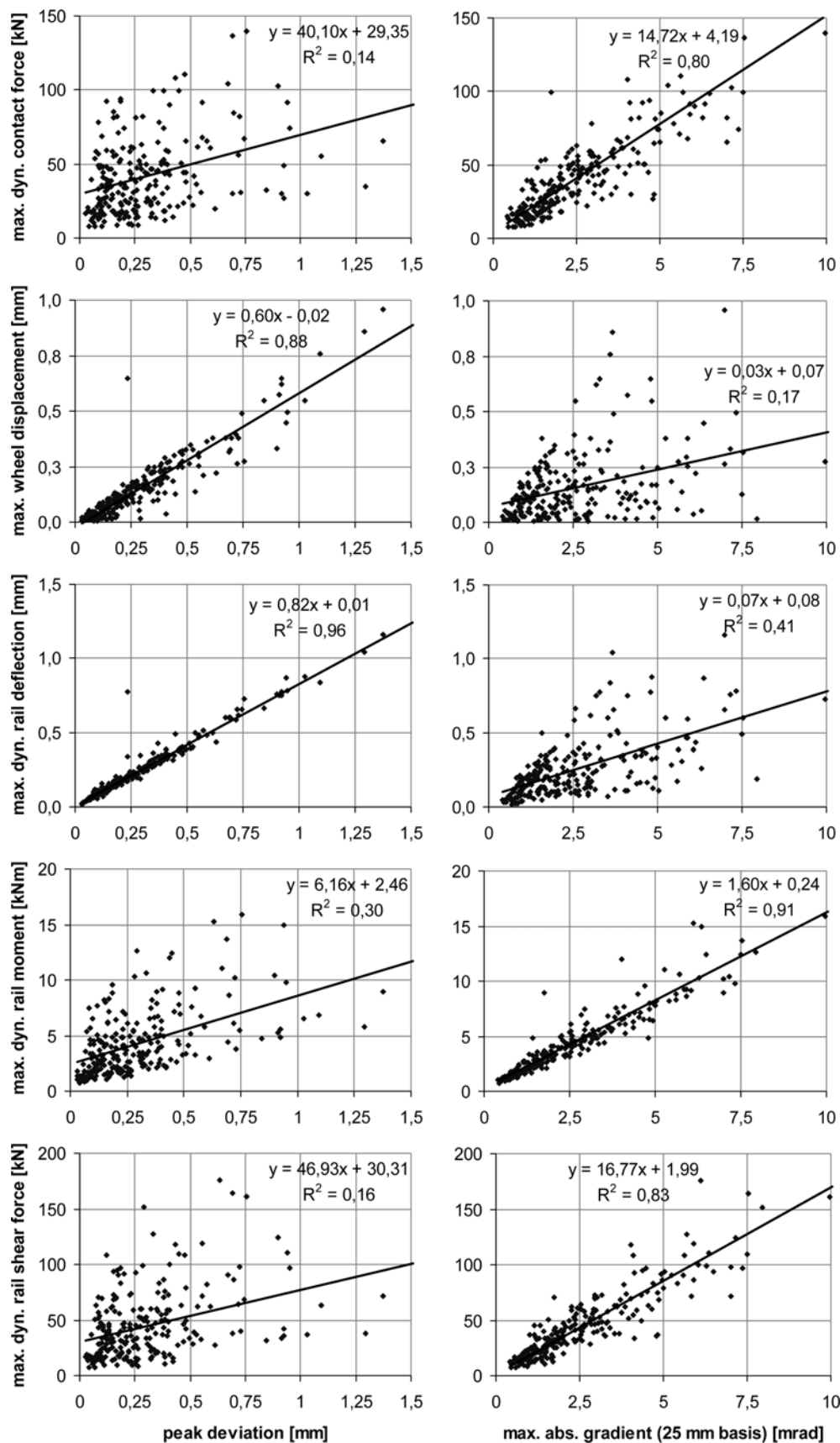
Fig. 10 Dynamic response of the wheel–rail system to rail welding irregularities for a train velocity of 300 km/h
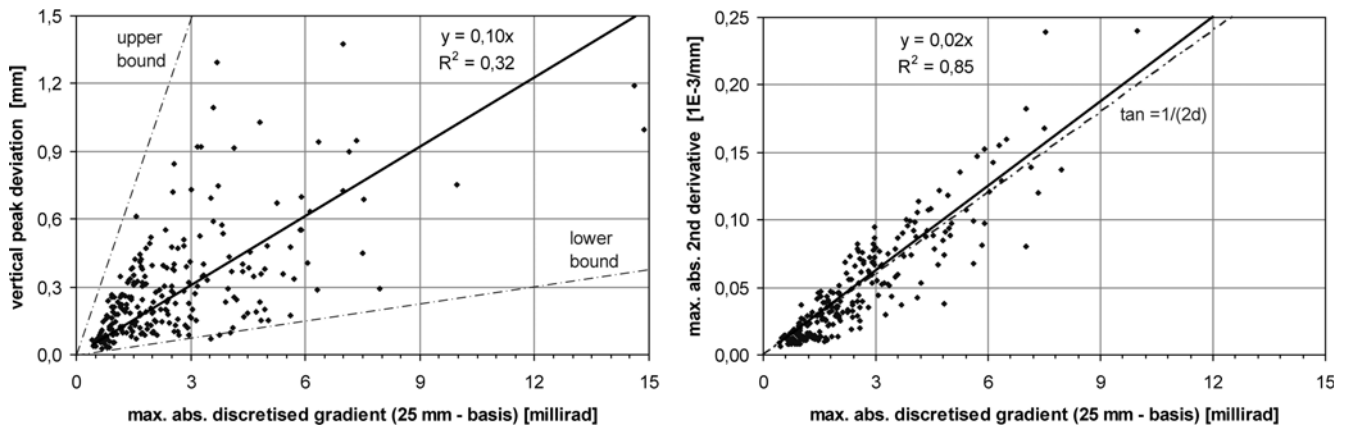
Fig. 11 Vertical peak deviations and maximum second derivatives in absolute sense, respectively, as a function of the maximum gradient in absolute sense of the measured welds (derivatives on 25 mm basis)

value of the discretized gradient, is given by (see reference [1], Fig. 12)

$$z_{max} = \tfrac{1}{4}L_{max}\left|\frac{dz}{dx}\right|_{max}, \qquad L_{max} = 2000 \text{ mm} \qquad (2)$$

The lower bound is given by

$$z_{min} = \tfrac{1}{4}L_{min}\left|\frac{dz}{dx}\right|_{max}, \qquad L_{min} = 100 \text{ mm} \qquad (3)$$

The exceptional excess of some values with respect to the lower boundary is due to the filtering and averaging processes of the original sampled signal, as pointed out in reference [1]. The wedge-shaped relationship between peak deviations and gradients can be easily recognized in several plots in Figs 7 to 10.

5 INFLUENCE OF THE VELOCITY ON THE RELATION BETWEEN FORCES AND RAIL WELD GRADIENTS

In reference [1], the following relationship has been derived theoretically

$$F_{dyn,\,max} = \gamma M_{track}V^2\frac{1}{d}\left|\frac{dz}{dx}\right|_{max} \qquad (4)$$

where $\gamma(-)$ is a dimensionless calibration factor (dependent on the line section speed interval); M_{track}(kg) the equivalent track mass; V(m/s) the train speed; d(m) the sampling distance in the averaged and filtered signals of the weld geometry (0.025 m), and $|dz/dx|_{max}$ (−) the intervention level for the gradient of this signal. The linear relationship between the gradient and the maximum dynamic contact force was confirmed by the analyses in the preceding section. The focus will now be on the relation between the maximum dynamic contact
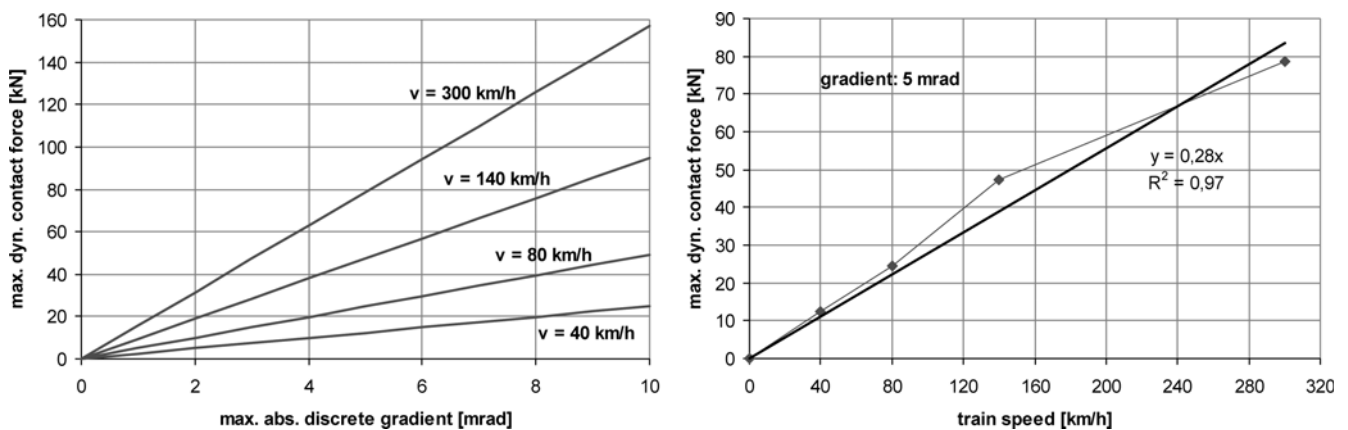

Fig. 12 Dependence of the dynamic wheel–rail contact forces at rail welds on the train velocity

force and the velocity, which according to equation (4) is quadratic.

In Fig. 12 at the left, the relation between the maximum dynamic wheel–rail contact force and the gradient (on 25 mm basis) is shown for the different velocities for which simulations were performed. For each velocity, a linear fit through the origin is displayed (which is not equal to the regression line); the equations of these fits are given by ($|dz/dx|_{max} = \tan \alpha$ and F_{dyn} in kN)

$$40 \, km/h: \quad F_{dyn} = 2.5 \tan \alpha \quad (5a)$$

$$80 \, km/h: \quad F_{dyn} = 4.9 \tan \alpha \quad (5b)$$

$$140 \, km/h: \quad F_{dyn} = 9.5 \tan \alpha \quad (5c)$$

$$300 \, km/h: \quad F_{dyn} = 15.7 \tan \alpha \quad (5d)$$

It should be remarked that the graphs in Fig. 12 show linear fits, disregarding any scatter in the results. Therefore, actual values may exceed the predicted values from Fig. 12, especially at low velocities (see Figs 7 to 10).

Figure 12 shows, at the right, the relation between the contact force and the train speed, given a certain gradient, which is taken as 5 mrad. It is observed that the influence of the velocity is not quadratic, as is predicted from equation (4). However, in general, the relation between the force and the speed can be well approximated as linear, yielding the following adapted relationship (4)

$$F_{dyn, max} = \gamma M_{track} V \frac{1}{d} \left| \frac{dz}{dx} \right|_{max} \quad (6)$$

The linear relationship between the maximum dynamic contact force (or the DAF) and the train speed is confirmed experimentally by the results of reference [3]. The linear relationship (6) between force, speed, and gradient allows combining equations (5) into the following approximate single equation, in terms of the variables V(m/s) and $|dz/dx|_{max}$ (=$\tan \alpha$) (mrad)

$$F_{dyn, max} = 0.22 \cdot V \cdot \tan \alpha \quad (kN) \quad (7)$$

It is observed that a similar result was found, both from simulations and experiments, by Jenkins *et al.* [5] in 1974 for the peak forces occurring at the dipped rail joints. The results were reflected in the well-known Jenkins' formula for the calculation of P_1 and P_2 forces [5]. They found these peak forces to be governed by the dip angle and the train speed; the relationship between maximum dynamic contact forces and both variables proved to be linear in a good approximation. Jenkins' results for rail joints, together with the results obtained for rail

welds, are shown in the graph of Fig. 13. In Fig. 13, peak forces for rail joints and welds are depicted as a function of the product of angle (or its tangent) and speed; α is defined as the angle of a dipped rail end with a horizontal line for rail joints, and as the maximum absolute value of the gradient (on 25 mm basis) of its geometry. It is observed that the force level for the rail welds is lower than that for the rail joints. This conforms with expectations and is partly explained by the quasi-static rail deflection, which is much larger for a jointed rail (which behaves as a hinged beam) than for a welded rail, under the same static axle load. This quasi-static deflection increases the dip angle at the moment of wheel passage.

6 CONSEQUENCES FOR STANDARDIZATION

In references [1] and [6], a proposal was made for the intervention levels of the gradient of the rail weld geometry for different track section velocity intervals. The proposed values were empirical. The present study allows for a validation of these values.

Equation (7) establishes the quantitative relationship between the maximum contact force, the maximum gradient of the weld geometry, and the train speed. In order to set speed-dependent norm values for the gradient consistently, a certain force level
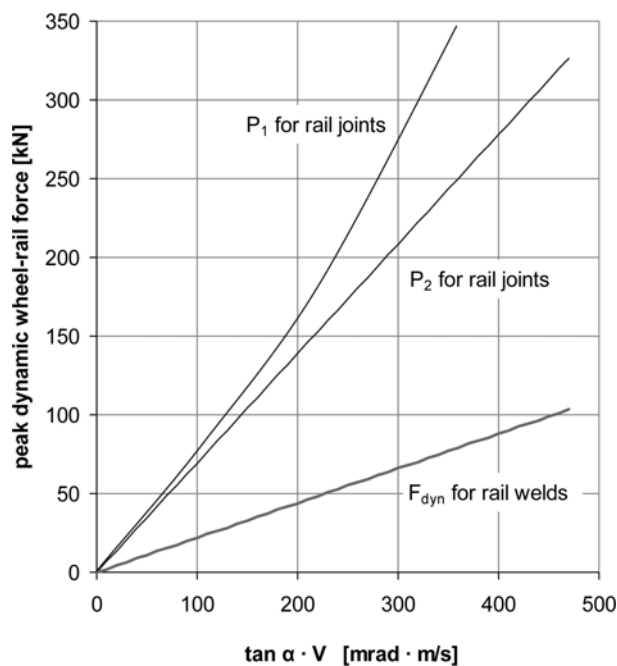

Fig. 13 Maximum dynamic wheel–rail forces for rail welds and rail joints as a function of the product of the maximum absolute gradient (on 25 mm basis) or the dip angle and the speed

should be admitted. This level should be coupled with the level of weld-related track deterioration; however, little is known regarding this relationship. Instead, two facts may be taken as a point of departure.

1. The empirical tolerance of 0.3 mm has been used worldwide for several decades, not leading to systematic problems. The maximum peak deviation following from the standardized gradient should, for 140 km/h (which is a regular passenger train speed), not be from a different order of magnitude.
2. The quality of the newly manufactured rail, after track laying but before track use, corresponds to a gradient of 0.7 mrad (as has been shown in reference [1]).

By adjusting the force levels at the different velocities conveniently to the dynamic force occurring for a high-speed train running at 300 km/h on a new rail (11 kN), the value of the dynamic wheel–rail contact force at the weld does not exceed the value at the rest of the rail. Using equations (5), the values are obtained, which are depicted in Fig. 14. The power fit to these values and the hyperbolic relationship (7) are also shown; they approximately coincide. In Fig. 14, the empirical values proposed in references [1] and [6] are also shown. It can be concluded that the values at 80, 200, and 300 km/h are very close to, or coincide with, the empirical values. However, the intervention values at 40 and 140 km/h are inconsistent. The intervention levels from reference [1] and the

curve-fitted newly calculated values are summarized in Table 1. In this table, the amplitudes of a sinusoidally shaped weld with half wavelength of 1 m are also given, giving an impression of the maximum possible tolerances according to the gradient values. At 140 km/h, this maximum amplitude equals 0.41 mm, which is of the same order of magnitude as the 0.3 mm mentioned earlier.

The values following from the calculations are based on the dynamic force level for new rail. It was shown in reference [1] that the corresponding norms for the geometry at 300 km/h are difficult to reach, even using a grinding train. Therefore, the norm may be 'relaxed', allowing a higher level of dynamic forces at the welds at all train velocities. In Fig. 14, the norm line in accordance with 'relaxation' of the force level with 100 per cent (which is an arbitrary number) is shown, being equivalent to an upward shift of the norm line with 0.7 mrad at 300 km/h. The corresponding values and the resulting tolerances for a harmonic wave with 2 m wavelength are given in the last two columns of Table 1. For repair works in existing tracks, where used rails must be joined mutually or to new rail parts, and where it is not possible to use the grinding trains, it may be necessary to use 'relaxed' values. A relaxation of 100 per cent is certainly an upper limit, according to the resulting possible peak deviations (last column of Table 1).

In Fig. 15, a comparison is made between the level of acceptation of welds according to the common
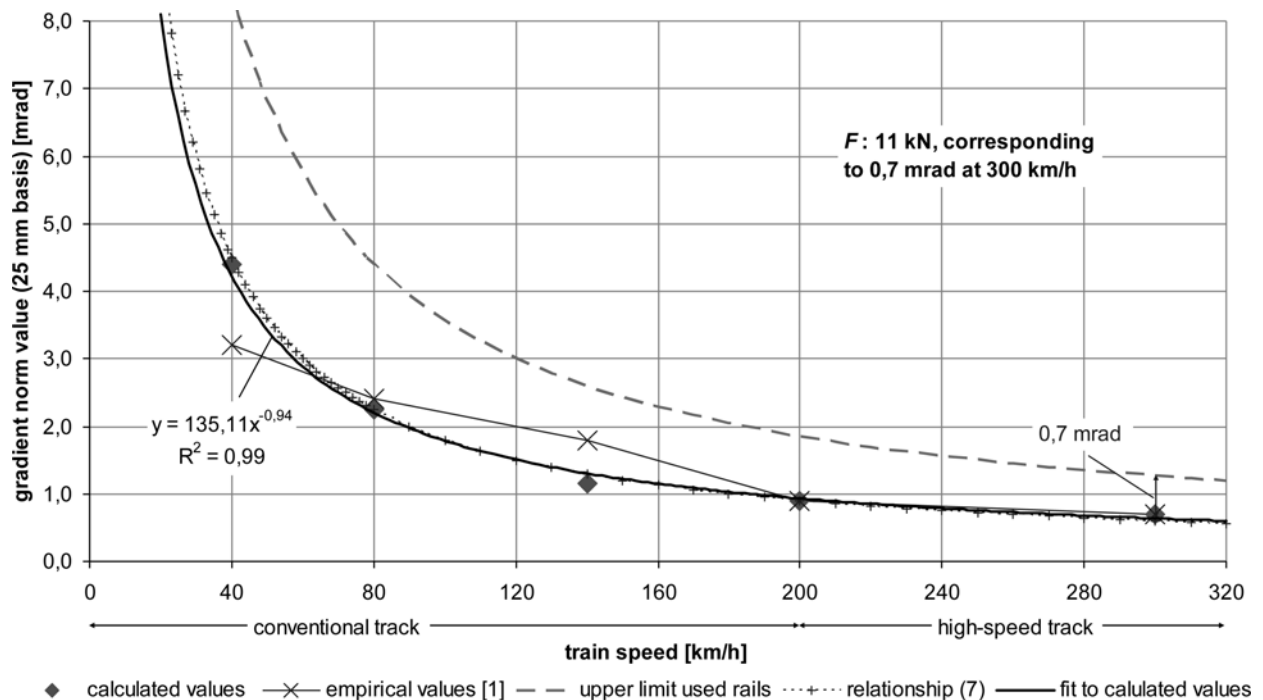

Fig. 14 Gradient norm values versus line section speed; empirical values proposed in reference [1], values following from the simulations and corresponding to the dynamic contact force for 0.7 mrad (new rail quality) at 300 km/h and relaxed values for used rails

Table 1 Norm values for maximum rail weld gradients to determine the rail weld QI

V(km/h)	Empirical values from [3] (mrad)	Resulting 2 m wave amplitude (mm)	Fit to calculated values; proposal for new rails (mrad)	Resulting 2 m wave amplitude (mm)	Relaxed values; upper limit for used rails (mrad)	Resulting 2 m wave amplitude (mm)
40	3.2	1.02	4.2	1.34	8.4	2.68
80	2.4	0.76	2.2	0.70	4.4	1.40
140	1.8	0.57	1.3	0.41	2.6	0.83
200	0.9	0.29	0.9	0.29	1.8	0.57
300	0.7	0.22	0.7	0.22	1.4	0.45

standards – based on vertical tolerances (0–0.3 mm, independent of the speed) – and the method based on gradients, in which the newly calculated values have been used (Table 1, fourth column). The analysis has been performed for a sample of 239 welds, which has been analysed in this article. It is observed that the acceptance level increases drastically, except for 300 km/h. At the common track section velocity of 140 km/h, the acceptance increases by 11 per cent. This is due to the fact that the peak deviations >0.3 mm are accepted, if the contact geometry is smooth. The percentages show that the newly validated values for new rail, although they seem very strict, are well acceptable.

7 FINAL CONSIDERATIONS AND CONCLUSIONS

The finite element (FE) model used in the simulations presented in this article models the rail as a Timoshenko beam. However, the beam model is incorrect for welding irregularities with a length scale shorter than the height of the rail. These irregularities lead to local dynamic forces which only penetrate into the railhead and do not lead to bending moments in the rail. For these cases, the beam model is not adequate and a more detailed FE model of the rail should be used in combination with a global track model, such as the model proposed by Ringsberg et al. [7–9] for investigating the local rail response. Especially, when the rail damage near the weld (fatigue and crack initiation) as a result of the dynamic amplification of the axle load is considered, it is important to account for the correct stress distribution along the height of the rail. This level of detail, which may be included in a later research, goes beyond the scope of the present research.

In the input for the simulations, the vertical geometry of the weld surface irregularities had a sampling interval of 5 mm (as in the real measurements). In the definition of QI, the interval of the averaged signal was extended to 25 mm, for practical reasons (especially manual grinding). The length of the wheel–rail contact patch is of the order of 5–20 mm. Slope transitions with a shorter basis do not lead to dynamic wheel–rail interaction, as they are covered by the contact area and disappear because of the plastic flow during wheel passage. The sensitivity of the level of the contact force to the sampling interval and the determination of the minimum basis of a transition in gradient which is 'felt' by the wheel–rail system are subjects of further research. In this article, the values 5 and 25 mm were used as boundaries of the region of interest for this basis. However, it can be mentioned in advance that a unique 'threshold' value for the length of the basis of the gradient below which the contact force does not change cannot be established, as it depends on the length of the Hertzian contact patch, which depends not only on the geometrical properties of wheel and rail, but also on the actual axle load.

In section 6, it was proposed to adopt 'relaxed' norm values for rail repair works on existing tracks; a 100 per cent relaxation was suggested as the upper limit. The actual percentage to be used should be determined from the relationship between the level of dynamic wheel–rail forces and the damage to the welded rail and the surrounding
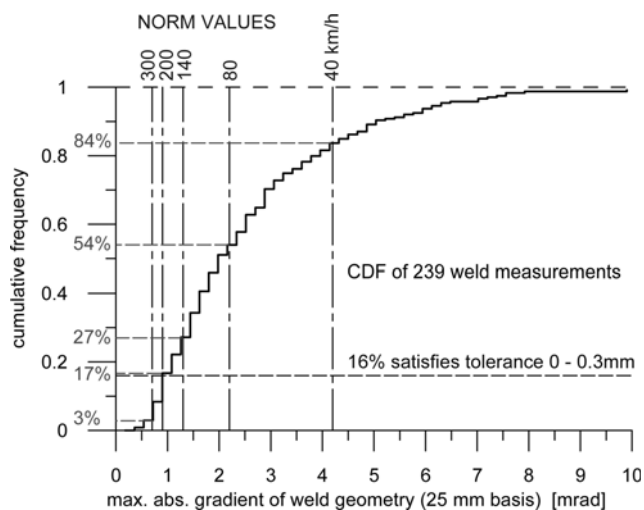

Fig. 15 Comparison of acceptation levels of rail welds for standardization methods based on vertical tolerances and gradients (according to Table 1, fourth column)

track. Further, the norm values were derived assuming a constant static axle load, whereas different axle loads of different train/track types may have an influence. These are subjects for further research, both theoretically and experimentally.

From this study, which considered the dynamic wheel–rail response to rail weld surface irregularities on a ballasted track, a number of conclusions can be drawn. They are as follows.

1. During the train wheel passage, the track follows a vertical rail weld surface irregularity quasi-instantaneously, whereas the wheel displacement shows a delay in response relative to the track. This phenomenon causes P_1 and P_2 wheel–rail forces.
2. The maximum dynamic contact force is determined by the irregularity with the shortest length scale. However, the corresponding force peaks are rather narrow and the corresponding amount of energy is rather small; these high-frequency peak forces damage mostly the rail itself.
3. The delayed reaction of the wheel mass results in a carrier frequency in the contact force. The highest amount of energy of the dynamic contact force is contained in this relatively low frequency. The relatively large energy contained in this carrier frequency is mainly responsible for the ballast bed deterioration, as it is not efficiently dissipated in the rail and the railpads.
4. There is no correlation between the maximum dynamic wheel–rail forces and the peak deviation of the vertical weld geometry. Therefore, an assessment based on the principle of peak deviations satisfying tolerances is inadequate to assess the geometry of rail welds from the viewpoint of dynamic wheel–rail forces and the resulting track deterioration.
5. The maximum gradient of the vertical weld geometry gives a good indication of the maximum dynamic wheel–rail forces occurring for a train wheel passing the weld. Therefore, the QI is a suitable tool to assess the rail weld geometry from a viewpoint of the dynamic wheel–rail response.
6. An approximate formula is derived, relating the maximum dynamic wheel–rail contact force at a weld irregularity linearly to the maximum gradient of the weld geometry and the train velocity. A similar (quasi-)linear relation between peak forces, train velocity, and dip angle has been established by Jenkins *et al.* for rail joints.
7. Norm values for the gradient of the longitudinal geometry of a weld have been derived depending on the line section train speed, allowing to determine the QI to assess the geometry of a rail weld [1]. These norm values lead to a uniform level of dynamic contact forces for all running speeds.

The present research is continued with an experimental study, in which the wheel–rail contact forces are measured for different types of welding irregularities and passing trains on real track. Preliminary test results were presented in reference [10].

ACKNOWLEDGEMENTS

REFERENCES

1 **Steenbergen, M. J. M. M.** and **Esveld, C.** Relation between the geometry of rail welds and the dynamic wheel–rail response: numerical simulations for measured welds. *Proc. IMechE, Part F: J. Rail and Rapid Transit*, 2006, **220**(F4), 409–423. (This paper.)
2 **Skyttebol, A., Josefson, B. L.,** and **Ringsberg, J. W.** Fatigue crack growth in a welded rail under the influence of residual stresses. *Eng. Fract. Mech.*, 2005, **72**, 271–285.
3 **Mutton, P. J.** and **Alvarez, E. F.** Failure modes in aluminothermic rail welds under high axle load conditions. *Eng. Fail. Anal.*, 2004, **11**, 151–166.
4 **DARTS-NL.** Dynamic analysis of a rail track structure, 2006, available from www.esveld.com.
5 **Jenkins, H. H., Stephenson, J., Clayton, G. A., Morland, G. W.,** and **Lyon, D.** The effect of track and vehicle parameters on wheel/rail vertical dynamic forces. *Rail. Eng. J.*, January 1974, 2–16.
6 **Steenbergen, M. J. M. M., Esveld, C.,** and **Dollevoet, R. P. B. J.** New Dutch assessment of rail welding geometry. *Eur. Rail. Rev.*, 2005, **11**, 71–79.
7 **Ringsberg, J. W., Bjarnehed, H., Johansson, A.,** and **Josefson, B. L.** Rolling contact fatigue of rails–finite element modelling of residual stresses, strains and crack initiation. *Proc. Instn Mech. Engrs, Part F: J. Rail and Rapid Transit*, 2000, **214**, 7–19.
8 **Ringsberg, J. W.** and **Josefson, B. L.** Finite element analyses of rolling contact fatigue crack initiation in railheads. *Proc. Instn Mech. Engrs, Part F: J. Rail and Rapid Transit*, 2001, **215**, 243–259.
9 **Ringsberg, J. W.** and **Lindbäck, T.** Rolling contact fatigue analysis of rails including numerical simulations of the rail manufacturing process and repeated wheel–rail contact loads. *Int. J. Fatigue*, 2003, **25**, 547–558.
10 **Esveld, C.** and **Steenbergen, M. J. M. M.** Force-based assessment of rail welds. In Proceedings of 7th World Congress on *Railway research*, Montreal, Canada, 4–8 June 2006.